Field-response of polymer microemulsions based on reactive mesogens

Ramesh Manda [a] , Surajit Dhara [a], Tae Hyung Kim [b], Young Jin Lim [c], Seung Hee Lee [b,c,d,*],
MinSu Kim [b,*]

[a] *School of Physics, University of Hyderabad, Hyderabad, Telangana 500046, India*
[b] *Department of Nano Convergence Engineering, Jeonbuk National University, Jeonju, Jeonbuk 54896, Republic of Korea*
[c] *Department of JBNU-KIST Industry-Academia Convergence Research, Jeonbuk National University, Jeonju, Jeonbuk 54896, Korea*
[d] *Department of Polymer Nano Science and Technology, Jeonbuk National University, Jeonju, Jeonbuk 54896, Republic of Korea*

ARTICLE INFO

ABSTRACT

Understanding molecular rearrangement of liquid crystals (LC) in microemulsions and manipulating their topology with external stimuli offer significant advantages for applications like sensors, displays, and smart windows. We fabricated monodisperse LC and reactive mesogen (RM)-LC microemulsions using porous glass membrane emulsification and investigated their topological transitions under electric fields. LC microemulsions retained their bipolar axes while responding to electric fields, whereas RM-LC microemulsions displayed a distinct response, where the polymer network rotated due to interfacial anchoring strength with field-responsive LCs, despite the polymer network's minimal dielectric anisotropy. These detailed findings on the RM-LC response highlight the role of interfacial interactions in structural transitions, facilitating the design of optimized topologies for low-power, high-performance optical devices.

1. Introduction

Emulsions are prevalent in soft matter sciences, and their responses to external stimuli have long been of interest. The formation of liquid crystal (LC) droplets and their transitions under electric fields are one of the widespread examples due to their broad array of applications, ranging from biosensors to light-absorbing materials and photonic devices [1–7]. Polymer-dispersed liquid crystals (PDLCs) are one of the most well-known examples for this application. The PDLC system is composed of LC and polymer, and fabrication of the PDLCs is usually including polymerization-induced phase separation (PIPS). The polymer matrix provides the surface for LC molecules anchored, which affects the orientation of bulk. Field driven-optical switching is allowed by changing the LC orientation. However, the three-dimensional interface gives high-operating voltage, which is one of the critical issues for practical applications.

The LC director *n*, which represents a group of molecules in similar direction, can vary with different LC droplet configurations depending on the surface. For instance, the homeotropic anchoring results in the formation of radial droplets (single hedgehog at the middle of the droplet), and the tangential or planar anchoring leads to the formation of bipolar droplets (two boojums on the surface). By controlling the droplet size and spatial positions of defects, which governs the topology of droplets, these droplets can be not only used in light shutters like PDLCs but also utilized for novel applications [4–6,8–12]. The director configurations can be controlled by the size of droplets, manipulating the boundary condition (surface anchoring) of droplets, and applying external cues like temperature, electric fields, and shear forces [13,14]. Notably, the LC droplets dispersed in an aqueous solution adsorb specific surfactants to alter their internal structure by modifying the anchoring force at the interface [3–5,15–19]. Here, topology manipulation by electric fields is a promising approach due to its easy integration property and high feasibility of controlling other parameters like temperature and surface energy [3,6,19–22]. The LC molecular orientation in the emulsions is determined by competition between elastic forces, surface energies, and electric potential energy. Recently, we reported the electric field-induced reorientation mechanism of micro-sized LC emulsions and how the individual emulsion can influence the optical state of the entire system [19]. Microemulsions are visible under polarized optical microscope (POM) to observe and understand the behavior of microemulsions for maximum applicability in various approaches, for example, nanosized RM-LC emulsions, which can be applied to light modulators and sensors due to its optically isotropic state compared to strongly scattered state of PDLCs.

---

* Corresponding authors at: Department of Nano Convergence Engineering, Jeonbuk National University, Jeonju, Jeonbuk 54896, Republic of Korea (S.H. Lee).
E-mail addresses: lsh1@jbnu.ac.kr (S.H. Lee), minsu.kim@jbnu.ac.kr (M. Kim).

Considering systems which contain bipolar droplets with the radius R_d and the LC director $\boldsymbol{n}_c$ in the center of the bipolar droplets with no electric field, the interface of droplets has anchoring coefficient W_d between LC and medium. When electric fields are applied, the free energy of the system can then be roughly described by elastic, surface, and dielectric free energy densities as follows [19,23],

$$f = \frac{KN}{2\pi R_d{}^2}(\boldsymbol{n}\cdot\boldsymbol{n}_c)^2 - \frac{W_d N}{4\pi R_d}(\boldsymbol{n}\cdot\boldsymbol{n}_d)^2 - \frac{\varepsilon_0 \Delta\varepsilon N}{2}(\boldsymbol{n}\cdot\boldsymbol{E})^2, \tag{1}$$

where K denotes approximated elastic constant of splay, twist, and bend deformation. The N, ε_0, and $\Delta\varepsilon$ are the number density of droplets, permittivity of vacuum, and the dielectric anisotropy of LCs. The $\boldsymbol{n}_d$ denotes the initial LC director near the surface within the droplets. In case of RM-LC in which RM is polymerized by UV irradiation, we need to consider polymer network within the droplets where LCs now interact with polymer network, which has additional anchoring coefficient W_p between LC and polymer network as follows,

$$f = \frac{KN}{2\pi R_p{}^2}(\boldsymbol{n}\cdot\boldsymbol{n}_p)^2 - \frac{W_d N}{4\pi R_d}(\boldsymbol{n}\cdot\boldsymbol{n}_d)^2 - \frac{3R_p{}^2 W_p N}{2R_d{}^3}(\boldsymbol{n}\cdot\boldsymbol{n}_p)^2 - \frac{\varepsilon_0 \Delta\varepsilon_p N}{2}(\boldsymbol{n}_p\cdot\boldsymbol{E})^2, \tag{2}$$

where R_p is the simplified radius of the cross section of the polymer network, implyng three-dimensional anchoring strength around the circumference of the polymer network at a cross section [23–25]. The interaction between LC and the droplet surface would be negligible. The $\boldsymbol{n}_p$ denotes the initial LC director around the polymer network. The elastic and anchoring free energy densities are arisen in competition where the LC director $\boldsymbol{n}$ differs from $\boldsymbol{n}_p$ based on the applied electric field.

Considering no polymer network, the electric field strength can then be deduced as,

$$E \approx \sqrt{\frac{1}{\varepsilon_0 \Delta\varepsilon R_d}\left(\frac{W_d}{2\pi} - \frac{K}{\pi R_d}\right)}. \tag{3}$$

In case of strong anchoring strength, $R_d \gg K/W$, we can neglect the surface term due to the elastic deformation at the surface with no electric field. In case $R_d \ll K/W$, the anchoring strength becomes meaningful to determine the threshold electric field strength [19]. With polymer network, we need to consider the R_p intead of R_d in which we consider the distance between polymer fibers would be in similar scale as the thickness of polymer fiber itself.

In this report, we fabricate polymer-LC droplets by using reactive mesogens (RMs) that can be photopolymerized, keeping their initial orientation. In this approach, the physical property of the RM-LC droplets can last longer than LC emulsions, and more importantly they can be simply rotated to change their optic axes (bipolar axes) based on low interfacial energy, so-called sliding interface between the polymer droplets and their medium. After fabricating monodispersed, micro-sized RM-LC droplets by a membrane emulsification technique (Shirasu Porous Glass (SPG) emulsifier), we explored how the electric field-dependent optical transition between LC emulsions and RM-LC emulsions are different.

2. Experimental section

We have fabricated microemulsions of LC and RM-LC by using a porous membrane emulsification technique (Shirasu Porous Glass (SPG) emulsifier). The LC microemulsion was fabricated by dispersing nematic LC, (MAT-07–1251, nematic to isotropic transition $T_{NI} = 68\,°C$, $n_e = 1.6442$, $n_o = 1.4950$, $\Delta n = 0.1492$ at 589 nm, dielectric anisotropy $\Delta\varepsilon = 30.1$ at 20 °C and 1 kHz, rotational viscosity $\gamma_1 = 279$ mPa·s, from Merck Performance Materials, Ltd.) into an aqueous continuous phase. The RM-LC microemulsion was fabricated by dispersing 60 wt% of HRM-1001–001 ($T_{NI} = 89\,°C$, $n_e = 1.6529$, $n_o = 1.5143$, $\Delta n = 0.1386$ at 589

nm, from Jiangsu Hecheng Display Technology Co., Ltd.), consisting of three chemicals (4-[[[4-[(1-Oxo-2-propenyl)oxy]butoxy]carbonyl]oxy] benzoic acid 2-methyl-1,4-phenylene ester, $\Delta\varepsilon = -1.8$, $\Delta n = 0.14$ (Fig. 9a); 2-methyl-1,4-phenylene bis(4-(3-(acryloyloxy)propoxy)ben-zoate), $\Delta\varepsilon = -1.8$ (Fig. 9b); 4-(*trans*-4-propylcyclohexyl)phenyl acrylate (Fig. 9c)) and 40 wt% nematic LC, MLC-2053 ($T_{NI} = 86\,°C$, $\Delta\varepsilon = 42.6$ at 1 kHz, $n_e = 1.7472$, $n_o = 1.5122$, $\Delta n = 0.235$ at 589.3 nm, splay $K_{11} = 13.2$ pN, twist $K_{22} = 6.5$ pN, bend $K_{33} = 18.3$ pN, $\gamma_1 = 123$ mPa·s from Merck Performance Materials, Ltd.), into aqueous medium. 1 wt% of photoinitiator (Irgacure-369, Sigma-Aldrich) was mixed in the RM-LC mixture. A homogenous mixture of RM and nematic LC were dispersed into the aqueous medium, which consist 5 wt% of polyvinyl alcohol (PVA, density 1.19–1.31 g/cm^2, melting point 200 °C, refractive index 1.477 at 632 nm, Sigma-Aldrich) through a glass membrane to obtain microemulsion. The ratio of LC or RM-LC to the medium was fixed at 50:50 for every sample. The PVA provides tangential anchoring of LC molecules and stabilizes droplets. The membrane emulsification conditions were as follows: membrane pore size 2 μm, stirring speed 600 rpm, sample temperature 50 °C, N$_2$ gas pressure 80 kPa. The schematic of SPG membrane emulsification is shown in Fig. S1a. More specifically, the dispersed phase pushes LC into the continuous phase through the rotating cylinder containing a porous membrane layer (Fig. S1b) under pressure applied. By controlling the speed of the continuous phase, pressure applied on the dispersed phase, and rotational speed of the cylinder, spherical-shaped and monodispersed LC and RM-LC droplets in water can be obtained on another side of the membrane. Typical director configurations of microemulsions, such as bipolar, radial, axial, and twisted structures, were illustrated in Fig. S1c. After characterization, the RM-LC microemulsion was polymerized by irradiated UV light of 10 mW/cm^2 for 60 min.

The obtained microemulsion samples were brush-coated on suitable substrates and performed structural and electrical characterizations. We have employed interdigitated patterned electrodes (6 μm and 16 μm electrode width and spacing, respectively), in-plane switching (IPS) cell, for these electrical characterizations [16,26]. The director configuration of LC and RM-LC droplets were determined by analyzing optical structures by POM (Eclipse E600 POL, Nikon) with a CCD camera (DXM 1200, Nikon). The field-dependent optical transition of microemulsions was analyzed by applying voltages. For vertical field application, two ITO substrates were attached by 30 μm cell gap. Square wave voltages at the frequency of 1 kHz were applied to the sample using a function generator (AFG3101C, Tektronix) and amplifier (FLC A400), and corresponding optical textures were recorded.

3. Results and discussions

3.1. Director profile of LC microemulsion

The corresponding optical images of LC microemulsions were taken as shown in Fig. 1a. We obtained stable monodispersed bipolar droplets with spatially distributed nematic directors $\boldsymbol{n}_c$, which would also represent the director orientation in the center of droplets. No indication of droplet coalescence and spatial movement were observed and the droplet size varies from 3.5 to 6.5 μm with a full-width half-maximum of 1.6 μm, as depicted in Fig. 1b. As the droplets show distinct textures due to random distribution of $\boldsymbol{n}_c$, we selected droplet-1 to 3 as shown in Fig. 1b and investigated their optical textures. Their possible director configurations were drawn as depicted in Fig. 1c (Section S2, Fig. S2). Contrary to the optical appearance, all these droplets exhibit a bipolar structure. The angle between $\boldsymbol{n}_c$ and one of the polarizers in droplet-1 to 3 were 43°, 3°, and 23°, respectively. Entire area appears bright in droplet-1 except for near boojums. The dark region is associated with the polarized light direction to $\boldsymbol{n}_c$.
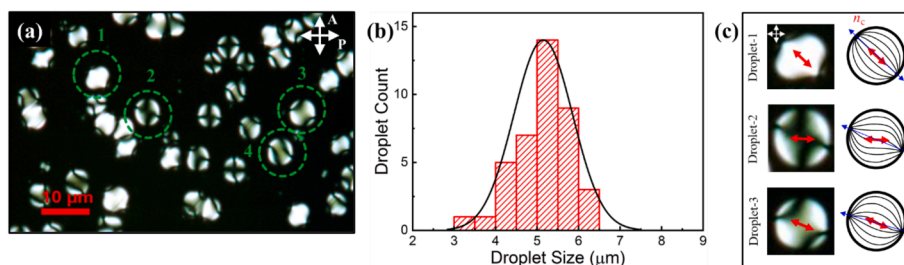
Fig. 1. (a) Optical micrographs of the obtained LC microemulsion. The selected droplets, droplet-1 to 3 are highlighted with green circles. (b) The droplet size distribution (histogram) and corresponding Gaussian fit of LC microemulsion. (c) The director profile and orientation of selected droplets. The white arrows indicate polarizer P and analyzer A, the blue arrows indicate bipolar axis, and the red arrows indicate LC director in the center of droplet n_c.

3.2. In-plane electric field-response of LC microdroplets

Elastic distortion of obtained nematic LC microemulsion droplets occurred and was investigated when applying in-plane electric field as shown in Fig. 2. The schematic representation of IPS and vertical field switching is schown in Fig. S3. The internal structure of the LC droplets and the orientation of n_c simultaneously changes along the applied electric field with no distortion of shape or size. The n_c rotation continues in the plane as the lateral field increases. Complete reorientation of the n_c was obtained at near 4.5 V/μm, and remarkably, the director in LC droplets is reversible after removing the applied field.

We observed LC droplets (droplet-2 to 4) for quantitative analysis of increase and decrease in the electric field strength. In Fig. 3a,d, the bipolar droplet-2 shows an angle φ between n_c and E is ~36°. The director configuration in the center of the droplets starts to deform, and the n_c rotated to align almost parallel to the electric field direction at 4.5–6 V/μm, which is common behavior of LC reorientation under electric fields, except that the reorientation shows thresholdless behavior at low electric field strength. On the other hand, the LC director in the vicinity of boojums still retained their initial orientation. A similar phenomenon was observed from droplet-3 (Fig. 3b,e) and 4 (Fig. 3c,f), which had its initial angle φ ~20° and 67°, respectively. In comparison among the droplets, the LC reorientation is relatively significant when the angle φ is larger. All droplets showed that, as the electric field was applied and released, the n_c completely turned back to the original direction, as droplet-4 was representatively shown in Fig. 3c,f. However, when φ is relatively smaller (in case of droplet-2 in Fig. 3d), the final reorientation angle, which is almost parallel to the direction of applied electric field, was reached at relatively lower electric field strength. In case φ is

relatively larger (in case of droplet-4 in Fig. 3f), the final reorientation angle is hard to reach as we arrange these values in Table 1. This implies each emulsion has their own different reorientation pathways, even if the whole cell measurement averages this effect.

As verified in the previous work [19], the LC director reorientation in the middle of droplets shows with no specific threshold electric field strength. We can estimate the threshold electric field strength from Eq. (3) when W_d (from 4×10^{-5} to 4×10^{-3} N/m, assuming $R_d = 6$ μm) and R_d (from 5 to 100 μm, assuming $W_d = 10^{-4}$ N/m) where $K_d = 10$ pN and $\Delta\varepsilon = 30$. We plotted the E_{th} as functions of R_d and W_d as shown in Fig. 3g. This plot shows E_{th} is below 0.3 V/μm in the range above mentioned, which suggests thresholdless behavior of the electric field strength, as the surface anchoring coefficient of PVA was measured in a previous report [27]. We may also understand that, when K and W_d are fixed and R_d is increased, E_{th} tends to reduce, meaning that the LC reorientation occurs relatively easily at larger droplet size. When K and R_d are fixed and W_d is increased, E_{th} tends to increase, meaning that at the same droplet size, higher anchoring strength makes the LC molecules seize under applied electric fields.

3.3. Vertical electric field-response of LC microdroplets

We also investigated reorientation mechanism under vertical electric fields as shown in Fig. 4 (Fig. S4). Increase in the electric field results in LC reorients at the center of the droplet first and it extends towards droplet surfaces. The vertical electric field response shows strong transmittance change. Most of the droplets become dark at 4.5 V/μm. The center of the droplet was completely darkened while slight light leakage remains near the surface. The droplets were further
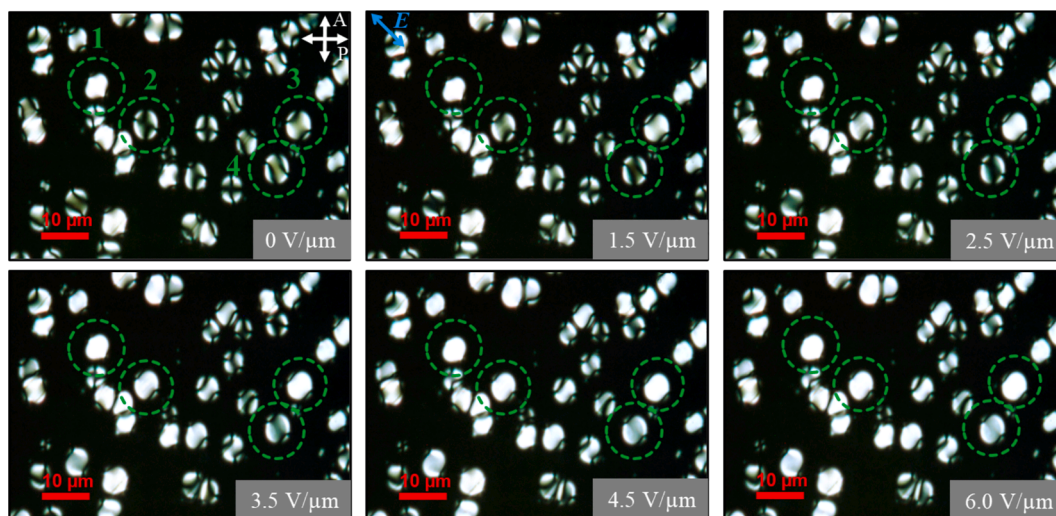

Fig. 2. Polarizing optical microscopy (POM) images of field-induced structural transition of LC droplets. The white arrows indicate polarizer P and analyzer A, the light blue arrow represents applied electric field E, and the scale bar is 10 μm.
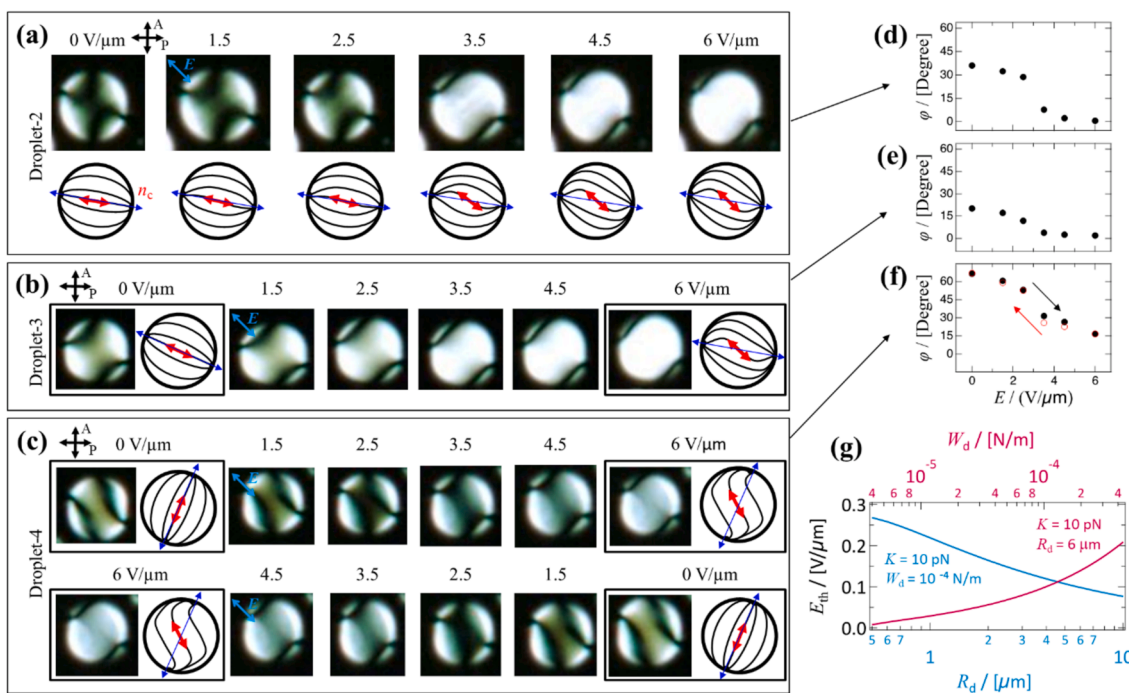
Fig. 3. Droplet configuration and field-dependent structural transitions of (a,d) droplet-2, (b,e) droplet-3, and (c,f) droplet-4. (a–c) POM images and corresponding droplet configurations. The black arrows indicate polarizer P and analyzer A, light blue arrows represents applied electric field *E*, the blue arrows indicate bipolar axis, and the red arrows indicate LC director in the center of droplet n_c. (d–f) Electric field strength-dependent reorientation of droplets-2 to 4, verified by the angle φ between the director field n_c and electric field direction. The black and red arrows in (f) indicate when electric field strength increases and decreases, respectively. (g) Estimation of the threshold electric field strength E_{th} as a function of the anchoring coefficient W_d and radius of droplets R_d.

Table 1

Electric field strength-dependent φ.

Angle between n_c and *E*	Droplet 2 (Fig. 3a,b)	Droplet 3 (Fig. 3c,d)	Droplet 4 (Fig. 3e,f)
φ_i (*E* = 0 V/μm) [°]	36	20	67
φ_f (*E* = 6 V/μm) [°]	1	2	17

characterized by additionally inserting a quarter-wave plate (QWP), as shown in Fig. S4. The introduction of quarter-wave retardation causes the droplet boundaries to appear in colors, even at 5 V/μm. This is due to the slight angular misalignment of LC molecules at boundaries resulting from strong interaction with the aqueous interface.

We observed three droplets with different directions of n_c as shown in Fig. 5a–c. Regardless of different LC director orientation, the reorientation was done at ~4.5 V/μm. The reorientation occurs without direction change in the bipolar axis of droplets at low electric fields, but near 4.0 V/μm, the direction of bipolar axis changes in plane. In the higher electric field strength, LC reorients even near the surface of droplets. The measured rise and decay response times of the whole cell under the vertical field were 0.5 and 1.5 s, respectively, which we believe are in similar range when under the in-plane field. These response times are averaged response times over many droplets so that it shows insufficient information for verifying individual droplet's response time. Although we categorized in-plane and vertical electric field responses in each section, each droplet's electro-optic responses are dependent on the vectorial relation between electric field direction and LC director field in droplets, which exist randomly oriented over the whole cell region. The reorientation pathways can vary due to the randomness of the LC director in droplets to the direction of electric field. Thus, we deduce the overall electro-optic response in plane and vertical electric fields would be in similar time.

3.4. Director profile of RM-LC microemulsion

We fabricated RM-LC microemulsions by keeping the experimental condition in Section 3.1. As POM images shown in Fig. 6a–c (Fig. S5), RM-LC bipolar droplets were produced with their average size of 8.8 μm and FWHM of 2.2 μm. The average size of the RM-LC emulsions is slightly bigger than the LC emulsions. The RM is pre-dissolved into the LC and then dispersed into the aqueous medium to fabricate microemulsion. Both RM and LC exhibit good dispersion and form stable microemulsions due to the mesophase and molecular similarity. The optical textures of RM-LC reveal the formation of randomly distributed bipolar droplets. There is no indication of shape and size deformation. The sample was rotated to 45° to estimate the structure of the droplet.

We selected RM-LC droplets and marked as droplet-1 to 8 with corresponding director profiles, illustrated as shown in Fig. 7 (Fig. S5). They were randomly distributed and freely suspended in a water medium before injecting in a cell. After injection, they settled down on the substrate at some point, resulting in random optical appearance. The bipolar axis of the droplet-1 and 2 lies on the plane of the substrate while the bipolar axis of the droplet-3 lies a long direction with azimuthal angle. The droplet-4 and 5 seem to have a twisted bipolar structure with a bipolar axis lying on the substrate plane and the droplet-6 and 7 have the bipolar axis out of the plane, whereas droplet-8 shows the bipolar axis in plane.

3.5. In-plane electric field-response of RM-LC microemulsions

The RM-LC microemulsions, consisting of 60 wt% of RM, were prepared by UV irradiation. The POM images show the transition of RM-LC under in-plane electric fields as shown in Fig. S6. The droplet structure and the spatial positions of boojums were observed by POM images with a quarter-wave plate inserted at 45° (Fig. S7). The POM images of droplet-1 in Fig. 8 show that the initial dark area moves towards the surface and finally occupies the area in the vicinity of boojums. The n_c is
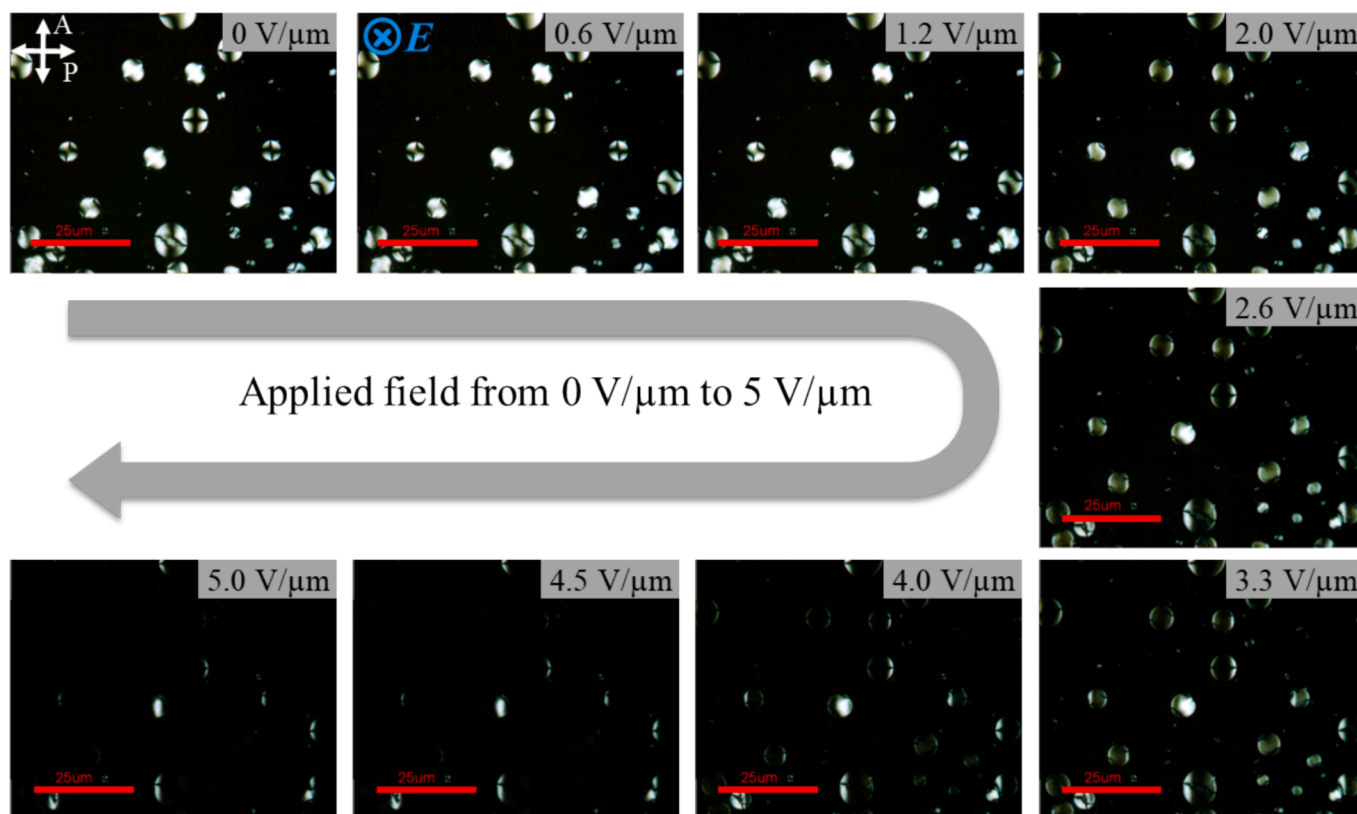
Fig. 4. Optical configuration of droplets under vertical electric fields. The white arrows indicate polarizer P and analyzer A, and the light blue cross in the circle represents applied electric field **E**. The scale bar is 25 μm.
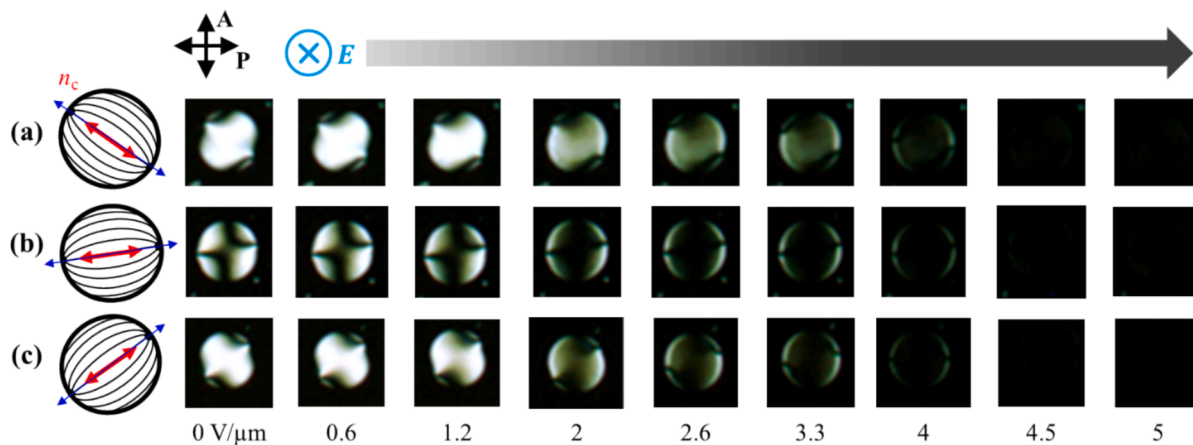

Fig. 5. POM images of vertical electric field response in bipolar droplets with different LC director orientation. The first column represents the initial director field. The black arrows indicate polarizer P and analyzer A, the light blue cross in the circle represents applied electric field **E**, blue arrows indicate bipolar axis, and the red arrows indicate LC director in the center of droplet **n_c**.

pre-aligned along the electric field, and then the LC molecules in the RM network are fully reoriented under 3 V/μm. The droplet-2 and 3 also exhibit similar trend. The azimuthal rotation of n_c is evident as the dark area in droplet-2 changes and finally disappears at 3 V/μm. From Fig. S7, the dark region of RM-LC droplets shown in Fig. 8 shows a color with QWP. Although it is a relatively indirect way to prove, the sharper boundary of different color caused by the QWP insertion implies different orientation of LC director whereas relatively blur boundary implies thicker polymer fibers.

To elucidate the underlying mechanism in the electric field-response of RM-LC droplets, we investigated the behavior of a RM-LC droplet,

which contains the matrix of polymerized RMs with their chemical structure shown in Fig. 9a–c. The LC molecules of 40 wt% coexist in the polymer network, which gives finite anchoring strength between them, and the optical appearance based on the director configuration is determined by the balance between anchoring strength and elasticity as shown in Fig. 9d. Here, it is necessary to consider the anchoring strength in the RM-LC droplet based on the interactions between LC and polymer network as described in Eq. (2). As the electric field strength increases, the reorientation in the center of the droplet occurred gradually as shown in Fig. 9e, which shows thresholdless behavior as verified in Fig. 3g. In Fig. 9f, the angle ω is between the bipolar axis (the location of
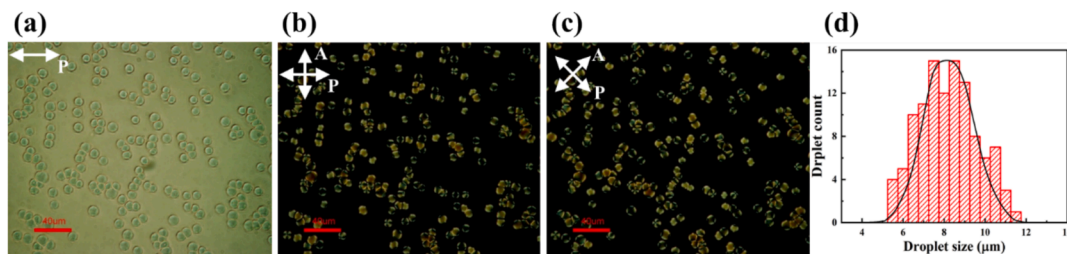
Fig. 6. RM-LC droplets. (a–c) Photomicrograph with (a) a single polarizer, (b) 0° and (c) 45° under one of the crossed polarizers. (d) Droplet size distribution and Gaussian fit. The white arrows indicate polarizer P and analyzer A, and the scale bar is 40 μm.
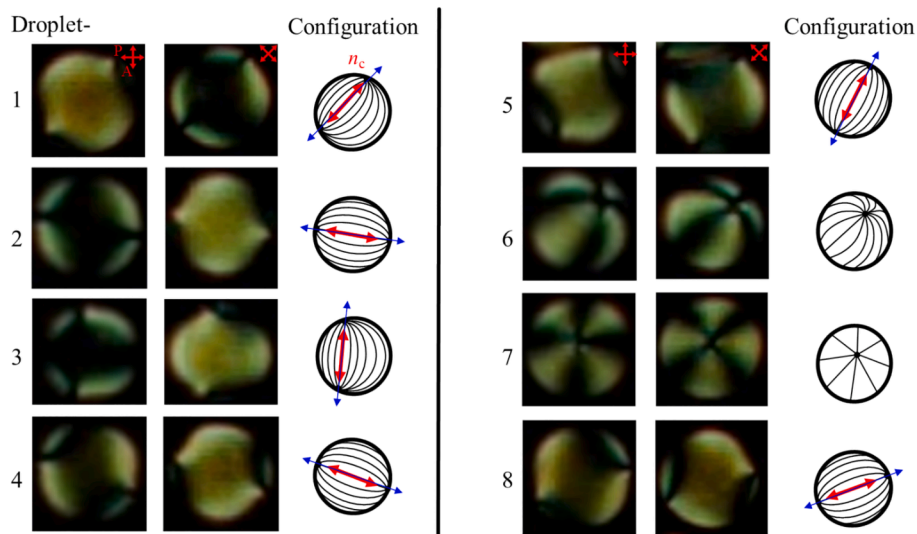

Fig. 7. POM images of RM-LC microemulsions (droplet-1 to 8) under crossed polarizers. The red arrows indicate polarizer P and analyzer A, the blue arrows indicate bipolar axis, and the red arrows indicate LC director in the center of droplet n_c.
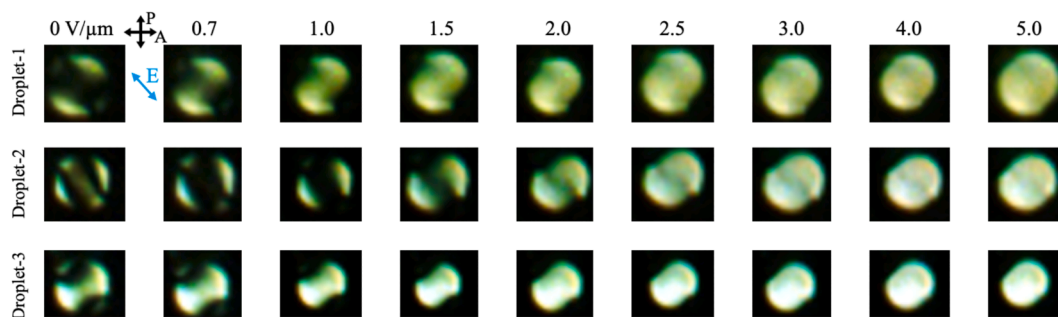

Fig. 8. POM images of structural evolution in RM-LC microemulsions under in-plane electric field. The black arrows are polarizers and the light blue arrow indicates the electric field direction.

boojums) and applied electric field direction. Unlike the LC reorientation, ω stayed until φ reaches the minimum at 4 V/μm. We discuss that the discrepancy $(\omega - \varphi)$ comes from the difference between dielectric anisotropy of LC and polymer network because the polymer network would have negative but relatively low dielectric anisotropy unlike the positive dielectric anisotropy in LC. (The individual RM moelcules in Fig. 9a–c have slight negative dielectric anisotropy, but it might be averaged out when polymerized.) Thus, the LC can follow their direction along the electric field over the certain electric field strength and reaches full alignment at 4 V/μm. Below 4 V/μm, the polymer network was not rotated until the dielectric energy exceeds the balance between elastic energy and anchoring strength between LC and polymer network. Upon decreasing the electric field strength, the bipolar axis of

polymer network was not fully turned back to the original location because of opposite dielectric anisotropy of LC and the polymer network. This result implies that the LC can easily follow the electric field direction due to the positive dielectric anisotropy, whereas the polymer network was not able to follow the electric field direction owing to the low negative dielectric anisotropy.

4. Conclusion

In this study, we developed LC and LC-polymer droplets and analyzed their reorientation under in-plane and vertical electric fields. The director configuration within the LC droplet is influenced by the elastic energy and the surface anchoring of the LC director to the droplet
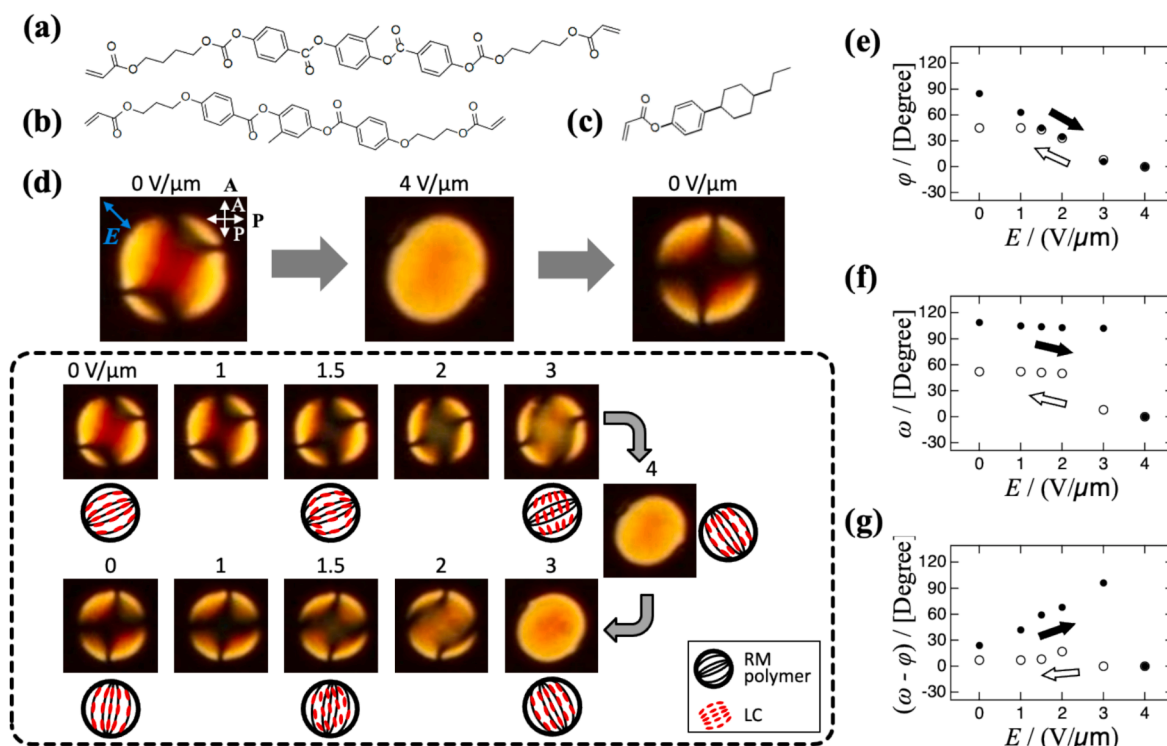
Fig. 9. The director response of a RM-LC droplet as the electric field strength increases and decreases. (a–c) Chemical structures of RM mixed in the RM-LC droplets. (d) POM images of the field-response of the RM-LC droplet. The white arrows indicate polarizer P and analyzer A, the light blue arrow represents applied electric field **E**. (e–g) Electric field strength **E**-dependent angles: (e) The angle φ between director orientation n_c and the electric field direction. (f) The angle ω between the bipolar axis and the electric field direction. (g) $(\omega - \varphi)$ with respect to the applied electric field strength. $(\omega - \varphi)$ represents difference in their angles of rotation of RM-LC droplets and LCs in the droplet. The solid and hollow markers indicate when **E** is increased and decreased, respectively.

surface. When an electric field is applied to LC bipolar droplets, the director profile undergoes a series of structural transitions before fully aligning with the electric field direction. The nature of these structural transitions depends on the alignment of the emulsions (including the bipolar axis in LC emulsions, and both the bipolar axis of the polymer fiber and the LC direction in RM-LC emulsions) relative to the electric field direction in three-dimensional space which we denoted φ between director orientation n_c and the electric field direction. When the initial orientation of the bipolar axis is already close to the final reorientation configuration, a lower electric field strength suffices to achieve the desired LC and RM-LC configuration.

In LC bipolar droplets, we observed director reorientation but no repositioning of boojums. Conversely, in RM-LC droplets, the LC reorients along the electric field direction, and subsequently, the polymer fiber (the bipolar axis) reorients once the field strength exceeds a certain threshold. Initially, changes in φ, the LC director field aligning with the electric field, occur without a threshold, as seen in LC droplets. However, changes in the angle ω between the bipolar axis and the electric field direction, the bipolar axis aligning with the electric field, indicate that the polymer fiber remains stable until the applied electric field strength surpasses 4 V/μm, at which point the fibers reposition to align with the field. When the field strength is reduced, both φ and ω return and relax, but ω does not fully revert to its original angle.

These findings demonstrate that polymer fibers with appropriate dielectric anisotropy can facilitate quicker bipolar axis rotation even in the absence of LC, enabling low-voltage rotation of the birefringent axis in polymer spheres. Additionally, the results provide insights into optical axis control at low voltages when fabricating nanoscale birefringent droplets, potentially enhancing light manipulation in devices such as light guides or sensors.

CRediT authorship contribution statement

Ramesh Manda: Writing – original draft, Visualization, Methodology. **Surajit Dhara:** Visualization. **Tae Hyung Kim:** Visualization. **Young Jin Lim:** Visualization. **Seung Hee Lee:** Writing – review & editing, Funding acquisition, Conceptualization. **MinSu Kim:** Writing – review & editing, Visualization, Methodology, Investigation.

Declaration of competing interest

The authors declare that they have no known competing financial interests or personal relationships that could have appeared to influence the work reported in this paper.

Acknowledgments

Appendix A. Supplementary data

Supplementary data to this article can be found online at https://doi.org/10.1016/j.molliq.2025.126849.

Data availability

Data will be made available on request.

References

[1] E. Brasselet, N. Murazawa, H. Misawa, S. Juodkazis, Optical vortices from liquid crystal droplets, Phys. Rev. Lett. 103 (2009) 103903, https://doi.org/10.1103/PhysRevLett.103.103903.

[2] S. Sivakumar, K.L. Wark, J.K. Gupta, N.L. Abbott, F. Caruso, Liquid crystal emulsions as the basis of biological sensors for the optical detection of bacteria and viruses, Adv. Funct. Mater. 19 (2009) 2260–2265, https://doi.org/10.1002/ADFM.200900399.

[3] S. Pagidi, R. Manda, H.S. Shin, J. Lee, Y.J. Lim, M.S. Kim, S.H. Lee, Enhanced electro-optic characteristics of polymer-dispersed nano-sized liquid crystal droplets utilizing PEDOT:PSS polymer composite, J. Mol. Liq. 322 (2021) 114959, https://doi.org/10.1016/J.MOLLIQ.2020.114959.

[4] S.L. Lee, M.S. Kim, D.Y. Lee, Y.H. Lin, S.H. Lee, Optically isotropic nano-size encapsulation of nematic liquid crystals with a high-filling factor, J. Mol. Liq. 359 (2022) 119254, https://doi.org/10.1016/J.MOLLIQ.2022.119254.

[5] S. Pagidi, H.S. Park, D.Y. Lee, M.S. Kim, S.H. Lee, Nanosize-confined nematic liquid crystals at slippery interfaces of polymer composites consisting of poly (hexyl methacrylate), J. Mol. Liq. 350 (2022) 118540, https://doi.org/10.1016/J.MOLLIQ.2022.118540.

[6] S. Pagidi, M.S. Kim, R. Manda, S. Ahn, M.Y. Jeon, S. Hee Lee, Ideal micro-lenticular lens based on phase modulation of optically isotropic liquid crystal-polymer composite with three terminals, J. Mol. Liq. 380 (2023), https://doi.org/10.1016/j.molliq.2023.121730.

[7] J. Jung, H.B. Park, H.Y. Jung, S.E. Jung, S.G. Kim, T.H. Kim, Y.J. Lim, B.C. Ku, M.S. Kim, S.H. Lee, Recent progress in liquid crystal devices and materials of TFT-LCDs, J. Inf. Display 25 (2024) 121–142, https://doi.org/10.1080/15980316.2023.2281224.

[8] L. Chen, H. Dai, G. Si, Y.J. Liu, B. Zhang, Optically isotropic, electrically tunable liquid crystal droplet arrays formed by photopolymerization-induced phase separation, Opt. Lett. 40 (2015) 2723–2726, https://doi.org/10.1364/OL.40.002723.

[9] S.A. Shvetsov, A.V. Emelyanenko, N.I. Boiko, J.H. Liu, A.R. Khokhlov, Communication: Orientational structure manipulation in nematic liquid crystal droplets induced by light excitation of azodendrimer dopant, J. Chem. Phys. 146 (2017) 211104, https://doi.org/10.1063/1.4984984.

[10] A. Concellón, D. Fong, T.M. Swager, Complex liquid crystal emulsions for biosensing, J. Am. Chem. Soc. 143 (2021) 9177–9182, https://doi.org/10.1021/jacs.1c04115.

[11] M.S. Kim, D.Y. Lee, H.Y. Jung, S.H. Lee, Superior photoluminescence of quantum dot displays via organic-inorganic composite scatterers, Compos. B Eng. 278 (2024) 111425, https://doi.org/10.1016/J.COMPOSITESB.2024.111425.

[12] L. Wang, H.K. Bisoyi, Z. Zheng, K.G. Gutierrez-Cuevas, G. Singh, S. Kumar, T.J. Bunning, Q. Li, Stimuli-directed self-organized chiral superstructures for adaptive windows enabled by mesogen-functionalized graphene, Mater. Today 20 (2017) 230–237, https://doi.org/10.1016/J.MATTOD.2017.04.028.

[13] M. Humar, M. Ravnik, S. Pajk, I. Muševič, Electrically tunable liquid crystal optical microresonators, Nat. Photonics 3 (2009) 595–600, https://doi.org/10.1038/nphoton.2009.170.

[14] Y. Zhou, E. Bukusoglu, J.A. Martínez-González, M. Rahimi, T.F. Roberts, R. Zhang, X. Wang, N.L. Abbott, J.J. De Pablo, Structural transitions in cholesteric liquid crystal droplets, ACS Nano 10 (2016) 6484–6490, https://doi.org/10.1021/ACSNANO.6B01088.

[15] M.S. Kim, L.C. Chien, Topology-mediated electro-optical behaviour of a wide-temperature liquid crystalline amorphous blue phase, Soft Matter 11 (2015) 8013–8018, https://doi.org/10.1039/c5sm01918d.

[16] R. Manda, S. Pagidi, M.S. Kim, C.H. Park, H.S. Yoo, K. Sandeep, Y.J. Lim, S.H. Lee, Effect of monomer concentration and functionality on electro-optical properties of polymer-stabilised optically isotropic liquid crystals, Liq. Cryst. 45 (2018) 736–745, https://doi.org/10.1080/02678292.2017.1380239.

[17] A.V. Dubtsov, S.V. Pasechnik, D.V. Shmeliova, A.S. Saidgaziev, E. Gongadze, A. Iglič, S. Kralj, Liquid crystalline droplets in aqueous environments: electrostatic effects, Soft Matter 14 (2018) 9619–9630, https://doi.org/10.1039/C8SM01529E.

[18] K. Nayani, U.M. Córdova-Figueroa, N.L. Abbott, Steering active emulsions with liquid crystals, Langmuir 36 (2020) 6948–6956, https://doi.org/10.1021/ACS.LANGMUIR.9B02975.

[19] M.S. Kim, R. Manda, D.Y. Lee, J.W. Lee, A. Nauman, H.R. Kim, S.H. Lee, Field-induced structural transitions in liquid crystal microemulsions, Adv. Opt. Mater. 10 (2022) 2200563, https://doi.org/10.1002/ADOM.202200563.

[20] E. Tjipto, K.D. Cadwell, J.F. Quinn, A.P.R. Johnston, N.L. Abbott, F. Caruso, Tailoring the interfaces between nematic liquid crystal emulsions and aqueous phases via layer-by-layer assembly, Nano Lett. 6 (2006) 2243–2248, https://doi.org/10.1021/nl061604p.

[21] G. Petriashvili, A. Chanishvili, T. Zurabishvili, K. Chubinidze, N. Ponjavidze, M.P. De Santo, M. Daniel, L. Bruno, R. Barberi, Temperature tunable omnidirectional lasing in liquid crystal blue phase microspheres, OSA Contin 2 (2019) 3337–3342, https://doi.org/10.1364/OSAC.2.003337.

[22] Y.J. Lim, M. Kang, H.S. Jeon, M.S. Kim, S.H. Lee, Low-temperature processable transparent liquid crystal light shutter, J. Mol. Liq. 368 (2022) 120823, https://doi.org/10.1016/j.molliq.2022.120823.

[23] P.S. Drzaic, Liquid crystal dispersions, World Scientific (1995), https://doi.org/10.1142/2337.

[24] M.S. Kim, Liquid Crystalline Amorphous Blue Phase: Tangled Topological Defects, Polymer-stabilization, and Device Application, 2015. http://rave.ohiolink.edu/etdc/view?acc_num=kent1448894363 (accessed March 16, 2022).

[25] P.G. de Gennes, J. Prost, The Physics of Liquid Crystals, Oxford University Press, 1995 https://global.oup.com/academic/product/the-physics-of-liquid-crystals-9780198517856?cc=kr&lang=en& (accessed August 10, 2021).

[26] J. Chen, W. Cranton, M. Fihn, Handbook of visual display technology, Handbook of Visual Display Technology 1–4 (2012) 1–2694, https://doi.org/10.1007/978-3-540-79567-4/COVER.

[27] Y. Cui, R.S. Zola, Y.C. Yang, D.K. Yang, Alignment layers with variable anchoring strengths from polyvinyl alcohol, J. Appl. Phys. 111 (2012) 063520, https://doi.org/10.1063/1.3697680.